Variational multiscale large eddy simulation of turbulent flows using a finite volume method

By V. Gravemeier

1. Motivation and objectives

The variational multiscale method represents a general approach for problems in computational mechanics which give rise to broad ranges of scales, see Hughes *et al.* (1998). The basic concept differentiates a predefined number of scale groups. This theoretical framework has also been applied to the problem of the incompressible Navier-Stokes equations in Hughes *et al.* (2000) in order to facilitate large eddy simulation (LES) of turbulent flows. In Collis (2001) and Gravemeier (2003), the variational multiscale method for LES has recently been broadened by raising the number of separated scale groups to three. Such a three-scale separation accounts specifically for large resolved scales, small resolved scales, and unresolved scales.

Apart from the initial separation and potentially different treatment of the respective scale ranges, two important aspects characterize the variational multiscale LES. Firstly, a variational projection separates scale ranges within the variational multiscale method rather than a spatial filter as in traditional LES. Secondly, the (direct) influence of the subgrid-scale model is confined to the small resolved scales. Thus, the large resolved scales are solved as a direct numerical simulation (DNS), i.e. without any (direct) influence of the modeling term. Of course, the large resolved scales are still influenced indirectly by the subgrid-scale model due to the inherent coupling of all scales.

At this stage, it should be pointed out that the variational multiscale method is essentially a theoretical framework for the separation of scales. Corresponding practical implementations within the variational multiscale framework are still rare. For such practical methods, it is crucial that a clear separation of the different scale ranges is actually achieved. The scale-separating approach developed in this work is implemented into the CDP-α code. Underlying this code is a finite volume method particularly suited for applications on unstructured grids. Please consult e.g. Ham *et al.* (2003) for further information concerning CDP-α. Within this computational environment, the separation of scales is developed in this work. A general class of scale-separating operators based on combined multigrid operators in a two-grid procedure is proposed here in order to replace spatial filters or their discrete analogs, respectively, which are widely used in classical LES. One particular representative of this class has the important property of a projector. A projector of this type has also been addressed in Koobus & Farhat (2004) as well as Vreman (2004).

The proposed methods of this work are applied to the case of a turbulent channel flow and compared to the DNS data in Moser *et al.* (1999). Turbulent channel flow has already served as one of the first test cases for variational multiscale LES in Hughes *et al.* (2001). That study was later complemented by Oberai & Hughes (2002) reporting the case $Re_\tau = 590$. A further study in Jeanmart & Winckelmans (2002) compares the subgrid-scale modeling approach of the variational multiscale method with other modeling approaches in the context of a turbulent channel flow. All of the aforementioned studies have one

important aspect in common: the use of a spectral method with higher-order accuracy in the homogeneous x_1-x_3-planes of the channel. In this work, the method applied is of second-order accuracy overall without any special treatment for the homogeneous planes of the channel. With regard to future applications in more complex geometries, performance of the variational multiscale LES within such a numerical environment is the more relevant test case, since spectral methods are by no means suited to such applications. The introduction of a generally larger numerical error due to the use of a second-order accurate method, combined with a relatively coarse discretization, has been investigated in Kravchenko & Moin (1997) at a high Reynolds number channel flow ($Re_\tau = 1000$). Similar evaluations have also been reported in Shah & Ferziger (1995) for a flow at very high Reynolds number $Re_\tau = 1800$ as well as in Terracol *et al.* (2001) for flows at Reynolds numbers $Re_\tau = 180$ and $Re_\tau = 590$.

This work basically follows the general guideline expressed in the idea that there exists an inherent link between, on the one hand, *physically motivated turbulence modeling* and, on the other hand, *numerically motivated modeling to account for inevitable errors due to an inadequate discretization*. A combined strategy relying on this observation has already been pointed out as a very promising tool in Collis (2001) and Gravemeier (2003). A detailed study of the approach to be presented in this work has recently been completed in Gravemeier (2004).

2. Variational three-scale formulation

A variational form of the incompressible Navier-Stokes equations reads

$$B_{NS}\left(\mathbf{v},q;\mathbf{u},p\right) = \left(\mathbf{v},\mathbf{f}\right)_\Omega \qquad \forall\left(\mathbf{v},q\right) \in \mathcal{V}_{\mathbf{u}p} \tag{2.1}$$

where $\mathcal{V}_{\mathbf{u}p}$ denotes the combined form of the weighting function spaces for velocity and pressure in the sense that $\mathcal{V}_{\mathbf{u}p} := \mathcal{V}_{\mathbf{u}} \times \mathcal{V}_p$. The bilinear form $B_{NS}\left(\mathbf{v},q;\mathbf{u},p\right)$ on the left hand side is hereby defined as

$$\begin{aligned} B_{NS}\left(\mathbf{v},q;\mathbf{u},p\right) = & \int_\Omega \mathbf{v}\frac{\partial \mathbf{u}}{\partial t}\,\mathrm{d}\Omega + \int_\Omega \mathbf{v}\nabla\cdot\left(\mathbf{u}\otimes\mathbf{u}\right)\,\mathrm{d}\Omega + \int_\Omega \mathbf{v}\nabla p\,\mathrm{d}\Omega \\ & - \int_\Omega \mathbf{v}\nu\Delta\mathbf{u}\,\mathrm{d}\Omega - \int_\Omega q\nabla\cdot\mathbf{u}\,\mathrm{d}\Omega \end{aligned} \tag{2.2}$$

where $\mathbf{v}$ and q denote the weighting functions. The L_2-inner product in the domain Ω on the right hand side is defined as usual:

$$\left(\mathbf{v},f\right)_\Omega = \int_\Omega \mathbf{v}f\,\mathrm{d}\Omega \tag{2.3}$$

The scales of the problem are now separated into three scale ranges as proposed in Collis (2001), Gravemeier (2003), and Gravemeier *et al.* (2004): the large resolved scales, small resolved scales, and unresolved scales. In terms of the underlying weighting and solution function spaces $\mathcal{V}_{\mathbf{u}p}$ and $\mathcal{S}_{\mathbf{u}p}$, this scale separation yields

$$\mathcal{V}_{\mathbf{u}p} = \overline{\mathcal{V}}_{\mathbf{u}p} \otimes \mathcal{V}'_{\mathbf{u}p} \otimes \hat{\mathcal{V}}_{\mathbf{u}p} \tag{2.4}$$

$$\mathcal{S}_{\mathbf{u}p} = \overline{\mathcal{S}}_{\mathbf{u}p} \otimes \mathcal{S}'_{\mathbf{u}p} \otimes \hat{\mathcal{S}}_{\mathbf{u}p} \tag{2.5}$$

According to this, the weighting functions read

$$\mathbf{v} = \overline{\mathbf{v}} + \mathbf{v}' + \hat{\mathbf{v}}; \quad q = \overline{q} + q' + \hat{q} \tag{2.6}$$

and, analogously, the solution functions are composed as

$$\mathbf{u} = \overline{\mathbf{u}} + \mathbf{u}' + \hat{\mathbf{u}}; \quad p = \overline{p} + p' + \hat{p} \tag{2.7}$$

Due to the linearity of the weighting functions, the variational equation (2.1) may now be decomposed into a system of three variational equations reading

$$B_{NS}\left(\overline{\mathbf{v}}, \overline{q}; \overline{\mathbf{u}} + \mathbf{u}' + \hat{\mathbf{u}}, \overline{p} + p' + \hat{p}\right) = \left(\overline{\mathbf{v}}, \mathbf{f}\right)_\Omega \qquad \forall \left(\overline{\mathbf{v}}, \overline{q}\right) \in \overline{\mathcal{V}}_{\mathbf{u}p} \tag{2.8}$$

$$B_{NS}\left(\mathbf{v}', q'; \overline{\mathbf{u}} + \mathbf{u}' + \hat{\mathbf{u}}, \overline{p} + p' + \hat{p}\right) = \left(\mathbf{v}', \mathbf{f}\right)_\Omega \qquad \forall \left(\mathbf{v}', q'\right) \in \mathcal{V}'_{\mathbf{u}p} \tag{2.9}$$

$$B_{NS}\left(\hat{\mathbf{v}}, \hat{q}; \overline{\mathbf{u}} + \mathbf{u}' + \hat{\mathbf{u}}, \overline{p} + p' + \hat{p}\right) = \left(\hat{\mathbf{v}}, \mathbf{f}\right)_\Omega \qquad \forall \left(\hat{\mathbf{v}}, \hat{q}\right) \in \hat{\mathcal{V}}_{\mathbf{u}p} \tag{2.10}$$

Furthermore, it is assumed that

$$B_{NS}\left(\overline{\mathbf{v}}, \overline{q}; \hat{\mathbf{u}}, \hat{p}\right) \approx 0 \tag{2.11}$$

relying on a clear separation of the large-scale space and the space of unresolved scales. Likewise, the opposite projection is assumed to be

$$B_{NS}\left(\hat{\mathbf{v}}, \hat{q}; \overline{\mathbf{u}}, \overline{p}\right) \approx 0 \tag{2.12}$$

This leads to a simplified equation system by changing (2.8) to

$$B_{NS}\left(\overline{\mathbf{v}}, \overline{q}; \overline{\mathbf{u}} + \mathbf{u}', \overline{p} + p'\right) = \left(\overline{\mathbf{v}}, \mathbf{f}\right)_\Omega \qquad \forall \left(\overline{\mathbf{v}}, \overline{q}\right) \in \overline{\mathcal{V}}_{\mathbf{u}p} \tag{2.13}$$

and (2.10) to

$$B_{NS}\left(\hat{\mathbf{v}}, \hat{q}; \mathbf{u}' + \hat{\mathbf{u}}, p' + \hat{p}\right) = \left(\hat{\mathbf{v}}, \mathbf{f}\right)_\Omega \qquad \forall \left(\hat{\mathbf{v}}, \hat{q}\right) \in \hat{\mathcal{V}}_{\mathbf{u}p} \tag{2.14}$$

whereas (2.9) remains unchanged.

It is not intended to resolve anything called unresolved *a priori*. Taking into account the effect of the unresolved scales onto the small scales is the only desire. Some alternatives lend themselves for this purpose as shown in Gravemeier (2003), but the focus here will be on the subgrid viscosity approach as a usual and well-established way of taking into account the effect of unresolved scales in classical LES. The small-scale equation (2.9) then reads

$$B_{NS}\left(\mathbf{v}', q'; \overline{\mathbf{u}} + \mathbf{u}', \overline{p} + p'\right) - \left(\mathbf{v}', \nu^T \Delta \mathbf{u}'\right)_\Omega = \left(\mathbf{v}', \mathbf{f}\right)_\Omega \qquad \forall \left(\mathbf{v}', q'\right) \in \mathcal{V}'_{\mathbf{u}p} \tag{2.15}$$

Due to assumption (2.11), the subgrid viscosity term directly acts only on the small resolved scales. Indirect influence on the large resolved scales, however, is ensured due to the coupling of the large- and the small-scale equations. Appropriate modeling approaches for the subgrid viscosity ν^T will be discussed in section 4. Note that the reason for introducing a model term in the variational formulation is mathematically different from the usual necessity of introducing a model term due to the appearance of a subgrid-scale stress tensor in the strong formulation of the Navier-Stokes equations in a classical LES. Nevertheless, the physical necessity to account for the missing effect of unresolved scales onto the resolved scales is the same in both cases.

The variational equations above may serve as the starting point for either a finite element formulation or a finite volume formulation, but the focus here is on the finite volume method. The presupposition for the application of the finite volume method is a discretization of the domain Ω into n_{cv} control volumes Ω_i $(i = 1, ..., n_{cv})$ with control volume boundaries Γ_i. The weighting functions are chosen to be

$$\mathbf{v}^h = \sum_i \mathbf{v}_i^h; \quad q^h = \sum_i q_i^h \tag{2.16}$$

where

$$\mathbf{v}_i^h = \mathbf{1}; \quad q_i^h = 1 \qquad \text{in} \quad \Omega_i \tag{2.17}$$

and zero elsewhere. In (2.17), $\mathbf{1}$ explicitly means that each component of $\mathbf{v}_i^h$ is of unit value. The characteristic control volume length of the discretization is h. With these definitions at hand, the variational equation (2.1) may likewise be formulated for each $\mathbf{v}_i^h$ and q_i^h such that

$$B_{NS}\left(\mathbf{v}_i^h, q_i^h; \mathbf{u}^h, p^h\right) = \left(\mathbf{v}_i^h, \mathbf{f}\right)_\Omega \qquad \forall \left(\mathbf{v}_i^h, q_i^h\right) \in \mathcal{V}_{\mathbf{u}p}^h \tag{2.18}$$

where the bilinear form on the left hand side is obtained from (2.2) after applying Gauss' theorem to the convective term, the pressure term, the viscous term, and the continuity term according to

$$\begin{aligned} B_{NS}\left(\mathbf{v}_i^h, q_i^h; \mathbf{u}^h, p^h\right) = & \int_\Omega \mathbf{v}_i^h \frac{\partial \mathbf{u}^h}{\partial t} \, \mathrm{d}\Omega + \int_{\Gamma_i} \mathbf{v}_i^h \left(\mathbf{u}^h \otimes \mathbf{u}^h\right) \cdot \mathbf{n} \, \mathrm{d}\Gamma + \int_{\Gamma_i} \mathbf{v}_i^h p^h \mathbf{n} \, \mathrm{d}\Gamma \\ & - \int_{\Gamma_i} \mathbf{v}_i^h \nu \mathbf{n} \cdot \nabla \mathbf{u}^h \, \mathrm{d}\Omega - \int_{\Gamma_i} q_i^h \mathbf{u}^h \cdot \mathbf{n} \, \mathrm{d}\Omega \end{aligned} \tag{2.19}$$

where Γ_i denotes the boundary of the support of $\mathbf{v}_i^h$ and q_i^h, respectively, and $\mathbf{n}$ the respective outward normal vector of unit length to this boundary of support.

The scale separation to be presented in section 3 relies on a level of complete resolution indicated by the characteristic control volume length h. In terms of the velocity, this reads

$$\mathbf{u}^h = \left(\overline{\mathbf{u}} + \mathbf{u}'\right)^h \tag{2.20}$$

With respect to this complete resolution level, a large-scale resolution level is identified *a priori*. This level is characterized by the control volume length $\overline{h}$ and, accordingly, yields a large-scale velocity $\overline{\mathbf{u}}^h$. The small-scale velocity is consistently defined as

$$\mathbf{u}'^h = \mathbf{u}^h - \overline{\mathbf{u}}^{\overline{h}} \tag{2.21}$$

Accordingly, a large-scale weighting function

$$\overline{\mathbf{v}}^{\overline{h}} = \sum_i \overline{\mathbf{v}}_i^{\overline{h}} \tag{2.22}$$

where

$$\overline{\mathbf{v}}_i^{\overline{h}} = \mathbf{1} \qquad \text{in} \quad \overline{\Omega}_i \tag{2.23}$$

and zero elsewhere is introduced. $\overline{\Omega}_i$ denotes the i-th control volume of the discretization with the characteristic control volume length $\overline{h}$. Reunifying the large-scale equation (2.13) and the small-scale equation (2.15) with the subgrid viscosity term on the basis of the preceding finite volume formulation yields a final equation which may be written in compact form with the help of (2.21) as

$$\begin{aligned} & B_{NS}\left(\mathbf{v}_i^h, q_i^h; \overline{\mathbf{u}}^h, p^h\right) - \left(\mathbf{v}_i'^h, \nu^T \mathbf{n} \cdot \nabla \mathbf{u}'^h\right)_{\Gamma_i'} \\ & = B_{NS}\left(\mathbf{v}_i^h, q_i^h; \overline{\mathbf{u}}^h, p^h\right) - \left(\mathbf{v}_i^h, \nu^T \mathbf{n} \cdot \nabla \left(\mathbf{u}^h - \overline{\mathbf{u}}^{\overline{h}}\right)\right)_{\Gamma_i} + \left(\overline{\mathbf{v}}_i^{\overline{h}}, \nu^T \mathbf{n} \cdot \nabla \left(\mathbf{u}^h - \overline{\mathbf{u}}^{\overline{h}}\right)\right)_{\overline{\Gamma}_i} \\ & = \left(\mathbf{v}_i^h, \mathbf{f}\right)_\Omega \qquad \forall \left(\mathbf{v}_i^h, q_i^h\right) \in \mathcal{V}_{\mathbf{u}p}^h; \quad \overline{\mathbf{v}}_i^{\overline{h}} \in \overline{\mathcal{V}}_{\mathbf{u}p}^{\overline{h}} \end{aligned} \tag{2.24}$$

where the boundary Γ_i is split up into a large-scale boundary $\overline{\Gamma}_i$ and, accordingly, a small-scale boundary subject to

$$\Gamma_i' = \Gamma_i - \overline{\Gamma}_i \tag{2.25}$$

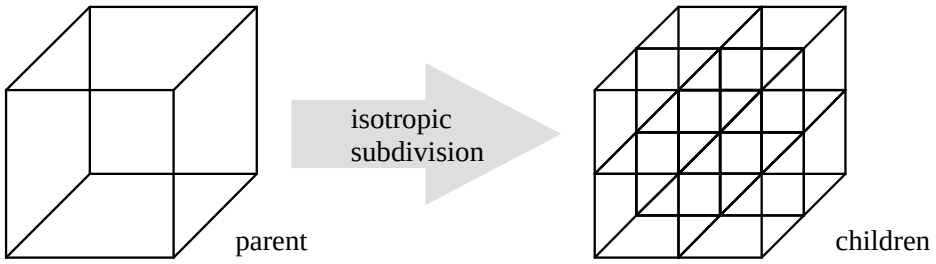

FIGURE 1. Parent hexahedron with 8 child hexahedra

These boundaries are illustrated in the figure at the end of the subsequent section. The inherent scale separation remains obvious in (2.24) merely due to the subgrid viscosity term.

3. Separation of scales

As a geometrical basis for the present approach, two grids are created: a coarser grid, which is called the 'parent' grid, and a finer grid, which is called the 'child' grid. The child grid is obtained by an isotropic hierarchical subdivision of the parent grid similar to the procedure described in Mavriplis (1997). In contrast to the usual parent-child relationship in multigrid solvers where the parent needs to know only the number of its children, a complete parent-child knowledge base is set up here, i.e. every parent knows about every child and vice versa. Hybrid unstructured meshes may contain tetrahedra, hexahedra, prisms, and pyramids. However, only two different types of faces, namely triangles and quadrangles, occur for these 4 different types of control volumes. Based on the fact that a factor of 2 is most often used in a dynamic modeling procedure for the relation of the cutoff length scale for the large resolved scales to the one for all resolved scales, an subdivision procedure using this factor is chosen. Both a parent triangular face and a parent quadrangular face subdivided isotropically result in four child faces of the same type. For the actual 3-D control volumes, isotropic subdivision of either a parent tetrahedron or hexahedron, for example, both results in 8 children. A parent hexahedron along with its 8 child hexahedra is depicted in Fig. 1. Illustrations of subdivided tetrahedra, prisms, and pyramids may be found in Mavriplis (1997). Obviously, this kind of refinement is not restricted to a subdivision by factor 2. Other integer factors (*e.g.*, 3 or 4) may be applied, and result in considerably lower ratios of the spaces containing the large resolved scales to the spaces containg the small resolved scales.

The general class of scale-separating operators based on multigrid operators reads

$$\overline{\mathbf{u}}^h = S^m\left[\mathbf{u}^h\right] = P \circ R\left[\mathbf{u}^h\right] = P\left[\overline{\overline{\mathbf{u}}^h}\right] \tag{3.1}$$

where the scale-separating operator S^m consists of the sequential application of a restriction operator R and a prolongation operator P. Applying the restriction operator on $\mathbf{u}^h$ yields a large-scale velocity $\overline{\overline{\mathbf{u}}^h}$ defined at the degrees of freedom of the parent grid which is then prolongated in order to obtain a large-scale velocity $\overline{\mathbf{u}}^h$ defined at the degrees of freedom of the child grid. Various restriction operators as well as prolongation operators may be used in (3.1). However, the attention is focused on two special combinations of restriction and prolongation operators. Both of them rely on the same restriction operator, but apply different prolongation operators afterwards. The restriction operator is

defined to be a volume-weighted average over all the child control volumes within one parent control volume subject to

$$\overline{\mathbf{u}}_j^{\overline{h}} = \frac{\sum_{i=1}^{n_{cop}} |\Omega_i| \, \mathbf{u}_i^h}{\sum_{i=1}^{n_{cop}} |\Omega_i|} \tag{3.2}$$

where $\overline{\mathbf{u}}_j^{\overline{h}}$ denotes the large-scale velocity at the center of the parent control volume $\overline{\Omega}_j$ and n_{cop} the number of child control volumes in $\overline{\Omega}_j$. The first prolongation operator P^p yields a constant prolongation, i.e.

$$\overline{\mathbf{u}}_i^h = P^p \left[\overline{\mathbf{u}}_j^{\overline{h}}\right]_i = \overline{\mathbf{u}}_j^{\overline{h}} \qquad \forall \Omega_i \subset \overline{\Omega}_j \tag{3.3}$$

and zero elsewhere. The scale-separating operator defined as

$$S^{pm} := P^p \circ R \tag{3.4}$$

has the property of a projector indicated by the additional superscript p. The second prolongation operator considered in this work yields a linear prolongation subject to

$$\overline{\mathbf{u}}_i^h = P^s \left[\overline{\mathbf{u}}_j^{\overline{h}}\right]_i = \overline{\mathbf{u}}_j^{\overline{h}} + \nabla^{\overline{h}} \overline{\mathbf{u}}_j^{\overline{h}} \, (\overline{\mathbf{r}}_j - \mathbf{r}_i) \qquad \forall \Omega_i \subset \overline{\Omega}_j \tag{3.5}$$

and zero elsewhere. The vectors $\mathbf{r}_i$ and $\overline{\mathbf{r}}_j$ denote geometrical vectors pointing to the centers of the child control voume Ω_i and the parent control volume $\overline{\Omega}_j$, respectively. $\nabla^{\overline{h}}$ describes the discrete gradient operator on the parent grid. Due to this, values from neighbouring parent control volumes and, consequently, child control volumes contained in these neighbouring parent control volumes influence the final large-scale value in the child control volume Ω_i. Hence, P^s does not provide us with a projective scale-separating operation as shown in Gravemeier (2004). It rather produces some kind of smoothing prolongation, which is indicated by the additional superscript s. The complete scale-separating operator is defined as

$$S^{sm} := P^s \circ R \tag{3.6}$$

Nevertheless, S^{sm} exhibits a fundamentally different character than usual discrete smooth filters.

The validity of (2.24) in a complete sense with respect to the subgrid viscosity term remains to be analyzed. In Gravemeier (2004), it is demonstrated that discrete smooth filters, in contrast to the scale-separating operators based on combined multigrid operators, do not satisfy (2.24) in a strict sense due to the fact that the third term in the second line of (2.24) cannot be represented. Nevertheless, there is also a crucial difference between S^{pm} and S^{sm} in this context: there is no large-scale (subgrid) viscous flux for S^{pm} across the small-scale boundary subject to (2.25), see Gravemeier (2004). As a result, (2.24) may be specified for S^{pm} as

$$B_{NS}\left(\mathbf{v}_i^h, q_i^h; \overline{\mathbf{u}}^h, p^h\right) - \left(\mathbf{v}_i'^h, \nu^T \mathbf{n} \cdot \nabla \mathbf{u}^h\right)_{\Gamma_i'} = \left(\mathbf{v}_i^h, \mathbf{f}\right)_\Omega \tag{3.7}$$

In Fig. 2, the definition of large- and small-scale boundaries in the finite volume method is visualized for the 2-D case. The large-scale weighting function $\overline{\mathbf{v}}^{\overline{h}}$ is exclusively defined on the large-scale boundaries belonging to the parent control volume as shown in Fig. 2(a). The small-scale weighting function $\mathbf{v}'^h$ is exclusively defined on the inner boundaries of the child control volumes, see Fig. 2(b).

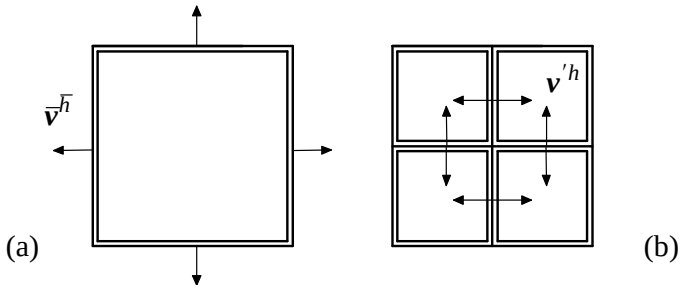

FIGURE 2. Geometrical locations of weighting functions in the FVM for a 2-D case: (a) large-scale; (b) small-scale

4. Subgrid-scale modeling within the multiscale environment

Adopting the usual filter-related notation for the Smagorinsky model to the underlying situation where the resolved part of the velocity is defined by the discretization with characteristic length scale h, the subgrid viscosity can be expressed as

$$\nu^T = (C_S h)^2 \left|\varepsilon\left(\mathbf{u}^h\right)\right| \tag{4.1}$$

The actual evaluation of (4.1) is performed in every control volume using the respective characteristic length scale, so that a value for ν^T in every control volume is obtained. Despite the well-known flaws of the constant-coefficient Smagorinsky, the integration of this simple model within the framework of the variational multiscale method has already led to good results for a number of test cases. The present study focuses on the specific modification of the model restricting the dependence on the small scales subject to

$$\nu^T = (C_S h)^2 \left|\varepsilon\left(\mathbf{u}'^h\right)\right| = (C_S h)^2 \left|\varepsilon\left(\mathbf{u}^h - \overline{\mathbf{u}}^h\right)\right| \tag{4.2}$$

which has been named 'small-small' model in Hughes *et al.* (2000) and seems to be the most natural version within the multiscale formalism. The constant C_S is chosen to be 0.1.

The dynamic modeling procedure proposed in Germano *et al.* (1991) enables a computation of the constant C_S as a function of time and position. It is interesting to note that the dynamic modeling procedure already distinguishes large resolved scales, small resolved scales, and unresolved scales explicitly. This mirrors the type of scale separation in the variational three-scale formulation.

Due to the pointwise formulation of the classical Germano identity, the dynamic procedure starts with a spatially discretized strong form of the Navier-Stokes equations. The spatially discretized momentum equation reads

$$\frac{\partial \mathbf{u}^h}{\partial t} + \nabla \cdot \left(\mathbf{u}^h \otimes \mathbf{u}^h\right) + \nabla p^h - \nu \Delta \mathbf{u}^h + \nabla \cdot \tau^h = \mathbf{f}^h \tag{4.3}$$

where the subgrid-scale stress tensor is defined as

$$\tau^h = (\mathbf{u} \otimes \mathbf{u})^h - \mathbf{u}^h \otimes \mathbf{u}^h \tag{4.4}$$

Note that in (4.3)-(4.4) the ususal filtered formulation is replaced by the actual implicit scale-separation based on the chosen discretization with characteristic length scale h. The 'test filter' is replaced by the scale-separating operators of section 3. Thus, the analog of the 'subtest'-scale stress tensor can be expressed as

$$\overline{\tau}^h = \overline{(\mathbf{u} \otimes \mathbf{u})}^h - \overline{\mathbf{u}}^h \otimes \overline{\mathbf{u}}^h = S\left[(\mathbf{u} \otimes \mathbf{u})^h\right] - S\left[\mathbf{u}^h\right] \otimes S\left[\mathbf{u}^h\right] \tag{4.5}$$

With regard to the child grid discretization level, the following may be stated:

$$\mathbf{L}^h = \overline{\tau}^h - \overline{\tau^h} = \overline{\tau}^h - S\left[\tau^h\right] \tag{4.6}$$

where $\mathbf{L}^h$ can be obtained as

$$\mathbf{L}^h = \overline{\mathbf{u}^h \otimes \mathbf{u}^h} - \overline{\mathbf{u}}^h \otimes \overline{\mathbf{u}}^h = S\left[\mathbf{u}^h \otimes \mathbf{u}^h\right] - S\left[\mathbf{u}^h\right] \otimes S\left[\mathbf{u}^h\right] \tag{4.7}$$

by inserting (4.4) and (4.5) into (4.6). Assuming the Smagorinsky model as an appropriate modeling term at both discretization levels and accounting for the fact that the Smagorinsky model is basically a 'trace-free' model in the context of incompressible flow, (4.6) is modeled as follows:

$$\begin{aligned} \mathrm{dev}\mathbf{L}^h &= \mathbf{L}^h - \frac{1}{3}\mathrm{tr}\mathbf{L}^h\mathbf{I} \\ &= -2\left(C_S h\right)^2 S\left|\left[\varepsilon\left(\mathbf{u}^h\right)\right]\right| S\left[\varepsilon\left(\mathbf{u}^h\right)\right] + S\left[2\left(C_S h\right)^2 \left|\varepsilon\left(\mathbf{u}^h\right)\right| \varepsilon\left(\mathbf{u}^h\right)\right] \end{aligned} \tag{4.8}$$

where $\mathbf{I}$ denotes the identity tensor, and modeling is obviously confined to the deviatoric part of the tensor $\mathbf{L}^h$. It is now assumed that C_S is at least constant over one control volume of the parent grid. Hence, (4.8) may be rewritten as

$$\begin{aligned} \mathrm{dev}\mathbf{L}^h &= \left(C_S h\right)^2 \left[2S\left[\left|\varepsilon\left(\mathbf{u}^h\right)\right| \varepsilon\left(\mathbf{u}^h\right)\right] - 2\left(\frac{\overline{h}}{h}\right)^2 S\left|\left[\varepsilon\left(\mathbf{u}^h\right)\right]\right| S\left[\varepsilon\left(\mathbf{u}^h\right)\right]\right] \\ &= \left(C_S h\right)^2 \mathbf{M}^h \end{aligned} \tag{4.9}$$

The calculation of the constant expression $\left(C_S h\right)^2$ on the right hand side of (4.9) aims to minimize the error tensor

$$\mathbf{E}^h = \mathrm{dev}\mathbf{L}^h - \left(C_S h\right)^2 \mathbf{M}^h \tag{4.10}$$

Using the least-squares approach proposed by Lilly (1992), the formula for the constant expression reads

$$\left(C_S h\right)^2 = \frac{\mathrm{dev}\mathbf{L}^h \mathbf{M}^h}{\mathbf{M}^h \mathbf{M}^h} \tag{4.11}$$

from which the actual constant C_S may be evaluated. Gravemeier (2004) discusses an alternative procedure based on the classical Germano identity which makes use of the special form of the scale-separating operators and yields only values for C_S related to the control volumes of the parent grid. The essential differences between this strategy and a new approach based on the so-called *variational Germano identity* of Oberai & Wanderer (2004) are also addressed.

5. Numerical example: turbulent channel flow

Three different methods are compared:

- the dynamic Smagorinsky (DS) model based on the classical Germano identity in the usual non-multiscale application,
- the constant-coefficient Smagorinsky (CMS) model in the 'small-small' version (4.2) within the multiscale environment subject to (2.24), and
- the dynamic Smagorinsky (DMS) model in the 'small-small' version (4.2) based on the classical Germano identity within the multiscale environment subject to (2.24).

All of these methods are investigated for the scale-separating operators S^{pm} and S^{sm}. The results are compared to simulations with discrete smooth filters based on the trapezoidal rule as well as the Simpson rule denoted S^{tf} and S^{sf}, respectively. In the following diagrams, the abbreviation DMS-PM, for instance, indicates the variational multiscale LES incorporating a dynamic Smagorinsky model with the scale-separating operator S^{pm} applied. Results are also reported for simulations using the constant-coefficient Smagorinsky model in a non-multiscale environment (CS) as well as applying no model at all (NM). It must be emphasized that CMS is merely the combination of these last two approaches by applying no model to the large resolved scales and the constant-coefficient Smagorinsky model to the small resolved scales.

Based on results of Gravemeier (2004), the characteristic length scale ratio for all DS and DMS simulations is set to 2.5 for S^{pm} and 2.0 for S^{sm}. For S^{tf} and S^{sf}, ratios of 2 and 1.5, respectively, are applied. The computational effort required for the various methodological combinations is also evaluated. In this brief, results are reported only for the case $Re_\tau = 590$ with a relatively coarse discretization of 64 control volumes in each coordinate direction. Gravemeier (2004) provides a detailed description of the numerical setup as well as the results for three other cases.

In order to compare the various methods, the scale-separating operator S^{pm} is used for DS, CMS, and DMS, since it is the most important operator of this work due to its projective property. Figs. 3 and 4 depict the mean streamwise velocity profile and the turbulent kinetic energy, respectively. The larger numerical error introduced by a second-order accurate method in combination with a relatively coarse discretization already mentioned in section 1 comes into play for all methods applied. Surprisingly however, the lower accuracy of the basic method affects CMS-PM to a far lesser extent than the other methods towards the channel center. It is considerably closer to the DNS profile in this part of the channel than NM, DS-PM, and DMS-PM. DMS-PM shows no improvement in comparison to NM, and DS-PM performs even slightly worse. Despite the higher accuracy in the inertial layer (usually expected to start at $x_2^+ = 30$), CMS-PM slightly underpredicts the velocity profile in the buffer layer (usually expected to range from $x_2^+ = 5$ to $x_2^+ = 30$). The profile for the turbulent kinetic energy shows a much better agreement for the height of the peak in comparison to the DNS profile than the other methods. Of course, CS is far worse than all other methods with respect to both aspects of the flow.

An objective comparison of the computational effort for the simulations using the aforementioned methods is difficult, since it strongly depends on the amount of computational time spent within the actual solvers in CDP-α. These time measures can vary considerably from one calculation to another. Thus, only approximate measures for the necessary computational effort are reported as a mean value of the actual simulation times covering all calculations in Gravemeier (2004). Setting the computational effort for NM to 1.0, the relative measures for CS, DS-PM, CMS-PM, and DMS-PM are circa 1.10, 1.15, 1.10, and 1.15, respectively. Thus, CMS in combination with PM is a very efficient method computationally, even more efficient than DS. Taking into account different scale-separating operators, the numbers increase drastically for CMS and DMS however.

A second important issue concerns the differences between the various scale-separating operators. In Figs. 5 and 6, the mean streamwise velocity and the turbulent kinetic energy, respectively, for four different scale-separating operators applied with DS, CMS, or DMS are pictured. There are hardly any differences visible for DMS in Fig. 5(c), but the scale-separating operators PM and SM perform better than TF and SF in the

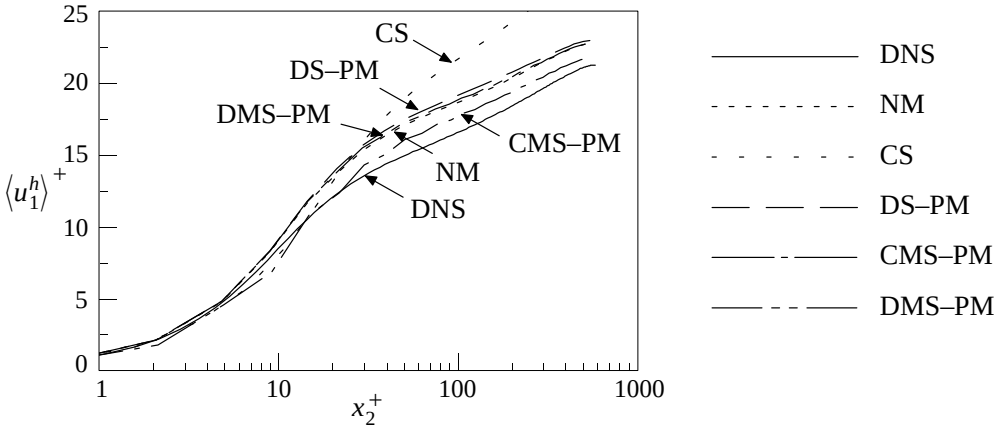

FIGURE 3. Comparing methods (pm-separation): mean streamwise velocity.

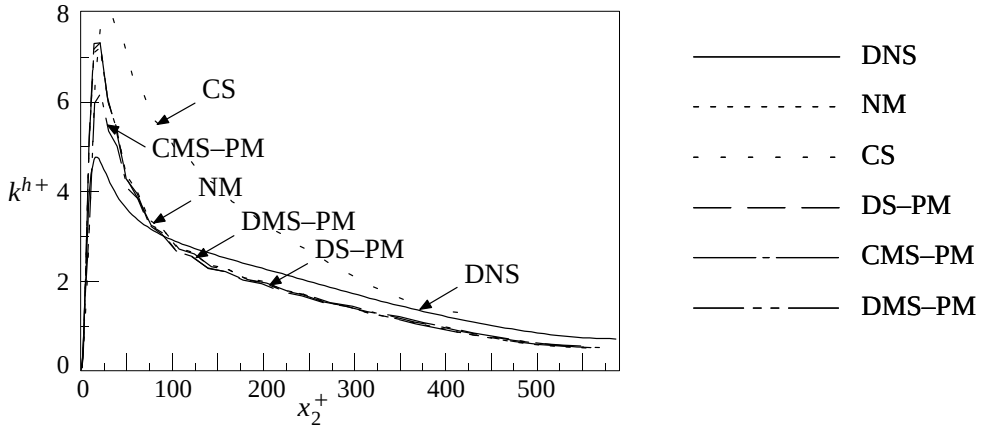

FIGURE 4. Comparing methods (pm-separation): turbulent kinetic energy.

context of DS, see Fig. 5(a). This presumption is, at least to a certain degree, reinforced for the turbulent kinetic energy profiles in Figs. 6(a) and (c). A remarkable difference between the projective scale-separating operator PM and the other operators shows up in the context of CMS for the mean streamwise velocity particularly as well as for the turbulent kinetic energy profile, although to a lesser degree, see Figs. 5(b) and 6(b). Thus, the favourable behaviour of CMS-PM in the inertial layer as well as the slightly underpredictive performance in the buffer layer and parts of the viscous sublayer seems to be attributed to CMS only depending on this specific scale-separating operator.

Specifying the necessary computational effort for the various scale-separating operators results in the following approximate numbers. Setting the relative computational simulation time for the operator PM to 1.0, the measures for SM, TF, and SF are approximately 1.25, 1.40, and 2.50, respectively. In particular, SF in this implementation is an extremely time-consuming operator and is, therefore, not recommended for further use. The reason for the additional effort linked with such non-projective operators can be traced back to a necessary call of the scale-separating routine at the beginning of each Gauss-Seidel iteration step in the solution procedure for the momentum equation.

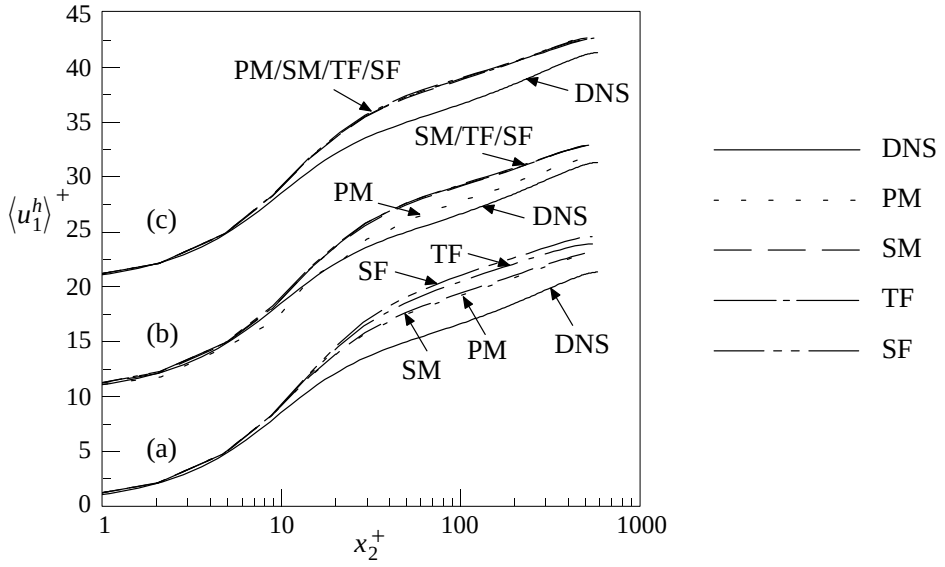

FIGURE 5. Comparing scale-separating operators: mean streamwise velocity: (a) DS; (b) CMS ($\langle u_1^h \rangle^+ +10$); (c) DMS ($\langle u_1^h \rangle^+ +20$).

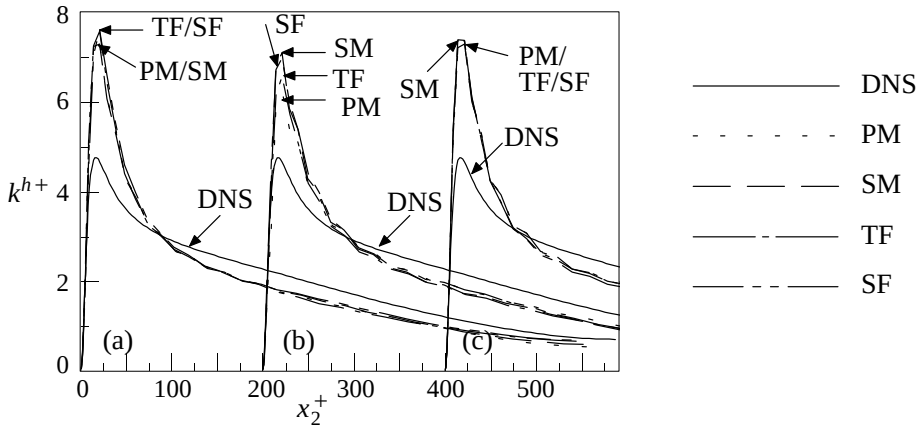

FIGURE 6. Comparing scale-separating operators: turbulent kinetic energy: (a) DS; (b) CMS ($x_2^+ +200$); (c) DMS ($x_2^+ +400$).

This call is required to determine the updated large-scale velocity field for the residual calculation. This is not necessary for PM.

In order to analyze the specific behaviour of CMS-PM in comparison to all other scale-separating operator in the context of CMS, the small scales are extracted and investigated explicitly in this section. Figs. 7 and 8 depict the mean streamwise small-scale velocity and the small-scale turbulent kinetic energy, respectively. The small-scale velocity of CMS-PM shows an oscillating behaviour with large amplitudes particularly in the buffer layer. For CMS-SM, the frequency of the oscillation is about the same, but the amplitudes are considerably smaller. In case of CMS-TF and CMS-SF, one oscillation period can be seen at most throughout half-width of the channel with the amplitude being larger for CMS-TF than for CMS-SF. As expected, the largest small-scale turbulent kinetic

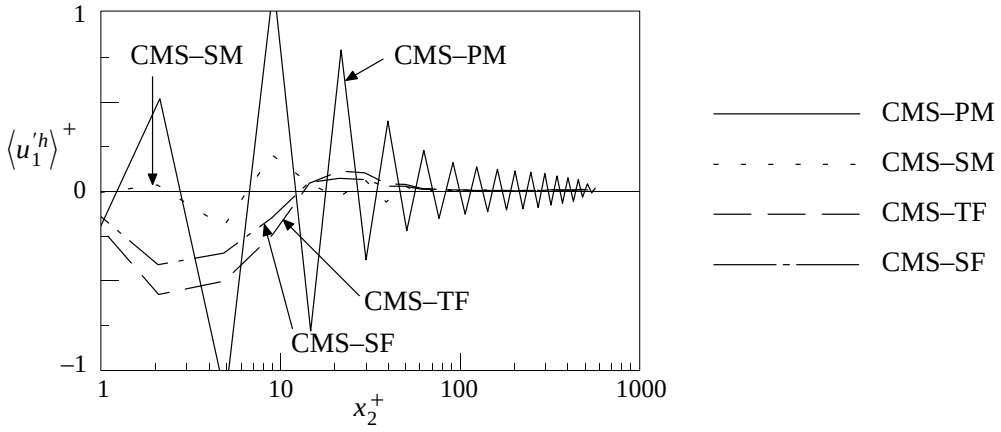

FIGURE 7. Comparing scale-separating operators for CMS: mean streamwise small-scale velocity.

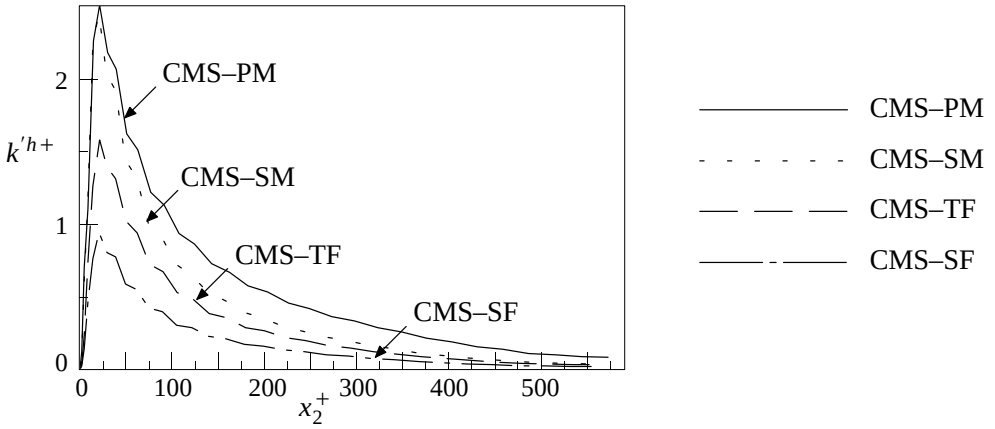

FIGURE 8. Comparing scale-separating operators for CMS: small-scale turbulent kinetic energy.

energy is obtained for CMS-PM (although the peak is also matched by CMS-SM) and the smallest one for CMS-SF, see Fig. 8. This indicates a measure for the amount of small scales extracted by the respective scale-separating operator and has been quantified in Gravemeier (2004).

6. Conclusions and future plans

A general class of scale-separating operators based on combined multigrid operators and suited for variational multiscale LES both with dynamic and constant-coefficient based subgrid-scale modeling has been proposed. These operators may also be used for the dynamic modeling procedure in a classical LES. Only one of these scale-separating operators exhibits the important property of a projector allowing fulfillment of the theoretical assumption for a clear scale separation within the variational multiscale method. All of the scale-separating operators have been implemented in a second-order accurate, energy-conserving finite volume method particularly suited for applications on hybrid unstructured grids in complex geometries. Dynamic and non-dynamic methods based on

the various scale-separating operators have been tested for the case of a turbulent channel flow at two different Reynolds numbers and for two different discretizations for each of these two Reynolds number flows. Several important observations have been made and summarized in Gravemeier (2004). With respect to certain crucial flow features, the simple constant-coefficient Smagorinsky model based variational multiscale method in combination with the projective operator has shown remarkable results. In particular, it represents a very efficient methodical combination with regard to the important aspect of computational cost.

Four subsequent projects growing from this study are currently underway or planned for the near future. First, the investigation of an alternative approach for dynamic subgrid-scale modeling based on the variational Germano identity is currently underway. In contrast to the classical Germano identity, this identity appears to be more consistent with the variational LES formulation. Second, the performance of the scale-separating operators based on combined multigrid operators will be investigated in the context of more challenging turbulent flows. These flow configurations will be characterized by an even larger range of subgrid scales than in the present investigation in order to provide an even more challenging test for variational multiscale LES. Currently, it is planned to use the turbulent flow in a planar asymmetric diffuser as such an additional test case. Third, the suitability of a more sophisticated approach for dynamic subgrid-scale modeling according to Ghosal *et al.* (1995) in the framework of variational multiscale LES will be investigated. Fourth, it is planned to address wall modeling approaches in this context.

7. Acknowledgements

The partial support by the Alexander von Humboldt-Foundation through a Feodor Lynen Fellowship is gratefully acknowledged. The author would like to express his sincere appreciation to Frank Ham for providing a basic version of the code CDP-α for the simulation of incompressible flows which the developments of this work are built upon. The author is also grateful to Parviz Moin and Gregory Burton for helpful discussions.

REFERENCES

Collis, S. S. 2001 Monitoring unresolved scales in multiscale turbulence modeling. *Phys. Fluids* **13**, 1800-1806.

Germano, M., Piomelli, U., Moin, P. & Cabot, W. H. 1991 A dynamic subgrid-scale eddy vicosity model. *Phys. Fluids* **3**, 1760-1765.

Ghosal, S., Lund, T. S., Moin, P. & Akselvoll, K. 1995 A dynamic localization model for large-eddy simulation of turbulent flows. *J. Fluid Mech.* **286**, 229-255.

Gravemeier, V. 2003 The variational multiscale method for laminar and turbulent incompressible fow. *PhD Thesis*, Report No. 40, Institute of Structural Mechanics, University of Stuttgart, Germany.

Gravemeier, V. 2004 Scale-separating operators for variational multiscale large eddy simulation of turbulent flows. *Preprint.*

Gravemeier, V., Wall, W. A. & Ramm, E. 2004 A three-level finite element method for the instationary incompressible Navier-Stokes equations. *Comput. Methods Appl. Mech. Engrg.* **193**, 1323-1366.

Ham, F., Apte, S., Iaccarino, G., Wu, X., Herrmann, M., Constantinescu,

G., MAHESH, K. & MOIN, P. 2003 Unstructured LES of reacting multiphase flows in realistic gas turbine combustors. *Annual Research Briefs - 2003*, Center for Turbulence Research, Stanford University and NASA Ames Research Center, 139-160.

HUGHES, T. J. R., FEIJOO, G. R., MAZZEI, L. & QUINCY, J.-B. 1998 The variational multiscale method - a paradigm for computational mechanics. *Comput. Methods Appl. Mech. Engrg.* **166**, 3-24.

HUGHES, T. J. R., MAZZEI, L. & JANSEN, K. E. 2000 Large eddy simulation and the variational multiscale method. *Comput. Visual. Sci.* **3**, 47-59.

HUGHES, T. J. R., OBERAI, A. A. & MAZZEI, L. 2001 Large eddy simulation of turbulent channel flows by the variational multiscale method. *Phys. Fluids* **13**, 1784-1799.

JEANMART, H. & WINCKELMANS, G. S. 2002 Comparison of recent dynamic subgrid-scale models in turbulent channel flow. *Proceedings of the Summer Program 2002*, Center for Turbulence Research, Stanford University and NASA Ames Research Center, 105-116.

KOOBUS, B. & FARHAT, C. 2004 A variational multiscale method for the large eddy simulation of compressible turbulent flows on unstructured meshes - application to vortex shedding. *Comput. Methods Appl. Mech. Engrg.* **193**, 1367-1383.

KRAVCHENKO, A. G. & MOIN, P. 1997 On the effect of numerical errors in large eddy simulations of turbulent flows. *J. Comput. Phys.* **131**, 310-322.

LILLY, D. K. 1992 A proposed modification of the Germano subgrid-scale closure method. *Phys. Fluids* **4**, 633-635.

MAVRIPLIS, D. J. 1997 Adaptive meshing techniques for viscous flow calculations on mixed element unstructured meshes. *ICASE-Report 97-20*, NASA Langley Research Center, Hampton, VA.

MOSER, R. D., KIM, J. & MANSOUR, N. N. 1999 Direct numerical simulation of turbulent channel flow up to $Re_\tau = 590$. *Phys. Fluids* **11**, 943-945.

OBERAI, A. A. & HUGHES, T. J. R. 2002 The variational multiscale formulation of LES: channel flow at $Re_\tau = 590$. *AIAA Paper 2002-1056*, Reno, NV, January 14-17, 2002.

OBERAI, A. A. & WANDERER, J. 2004 A dynamic approach for evaluating parameters in a numerical method. *Preprint*, submitted for publication in Int. J. Numer. Meth. Engrg.

TERRACOL, M., SAGAUT, P. & BASDEVANT, C. 2001 A multilevel algorithm for large-eddy simulation of turbulent compressible flows. *J. Comput. Phys.* **167**, 439-474.

SHAH, K. B. & FERZIGER, J. H. 1995 A new non-eddy viscosity subgrid-scale model and its application to channel flow. *Annual Research Briefs - 1995*, Center for Turbulence Research, Stanford University and NASA Ames Research Center, 73-90.

VREMAN, A. W. 2004 The adjoint filter operator in large-eddy simulation of turbulent flow. *Phys. Fluids* **16**, 2012-2022.